Pressure-induced structural and electronic phase transitions in GaGeTe

Amit Pawbake,[1,*] Christophe Bellin,[2,*] Lorenzo Paulatto,[2] Deepa S. Narang,[3] Keevin Béneut,[2] Benoit Baptiste,[2] Paola Giura,[2] Johan Biscaras,[2] Federico Alabarse,[4] Dattatray J. Late,[5] Otakar Frank,[1] and Abhay Shukla[2,†]

[1]*J. Heyrovský Institute of Physical Chemistry of the Czech Academy of Sciences, Dolejškova 2155/3, CZ-182 23 Praha, Czech Republic*

[2]*Institut de Minéralogie, de Physique des Matériaux et de Cosmochimie, Sorbonne Université, UMR CNRS 7590, MNHN, IRD UMR 206, 4 Place Jussieu, F-75005 Paris, France*

[3]*Department of Physics, Indian Institute of Science, Bangalore 560012, Karnataka, India*

[4]*Elettra Sincrotrone Trieste, S.C.p.A., I-34149 Basovizza, Trieste, Italy*

[5]*MST, Brane Enterprises Private Ltd, Hyderabad 500081, India*

(Received 28 January 2022; revised 22 December 2023; accepted 25 January 2024; published 15 February 2024)

Chalcogenide-based compounds are an important part of the family of layered materials, extensively studied for their two-dimensional properties. An interesting line of investigation relates to the evolution of their properties with hydrostatic pressure, which could lead to structural transitions and itinerant electronic behavior. Here, we investigate the evolution of a layered ternary compound GaGeTe as a function of pressure with x-ray diffraction, Raman and infrared spectroscopy, and *ab initio* calculations. The Ge layer retains a germanenelike vibration though enveloped in Ga and Te layers. We show experimental and theoretical evidence of metallization in two steps. At ∼6 GPa Raman and infrared spectroscopic data undergo changes compatible with delocalized charge carriers. Calculations ascribe this to the Fermi-level crossing of a valence band. At ∼16 GPa infrared transmission and Raman modes disappear and x-ray diffraction signals a structural transition to a phase which is metallic according to our calculations. We obtain consistent agreement between experiment and theory concerning the structural, vibrational, and electronic structure evolution with pressure.

DOI: 10.1103/PhysRevB.109.054107

I. INTRODUCTION

In layered chalcogenide compounds, a variation of the metal and the chalcogenide species allows for a wide range of properties and structures. Gallium germanium telluride (GaGeTe), a ternary compound, is of interest because of possible topological states which may exist in view of the eventual small band gap in its electronic structure [1,2]. The rhombohedral $R\bar{3}m$ structure of GaGeTe consists of hextuple layers (Te-Ga-Ge-Ge-Ga-Te) bound by van der Waals interactions. In each layer, the Ge atoms form a buckled hexagonal sheet. The buckling is substantial and this atomic plane can also be visualized as a double Ge layer in the armchair configuration. The Ge plane is sandwiched by two GaTe layers with the β-GaSe structure. This suggests that GaGeTe may actually be a natural germanene analog packaged in GaTe. However, the layers cleave at the Te-Te interface which implies that Ge-Ga bonds are relatively strong. An interesting direction is to study the evolution of the GaGeTe structure and electronic states as a function of pressure as has been done for layered materials such as MoS_2 [3,4] or BiTeI [5] in the recent past. Some questions that are pertinent for GaGeTe include the following. Can metallization be observed with pressure? Are there structural phase transitions with pressure? We examine the pressure phase diagram of GaGeTe with Raman and IR spectroscopy, synchrotron x-ray diffraction (XRD), and *ab initio* calculations. A zone center Raman mode [6] linked to the in-plane vibrations of germanium atoms does exist with E_g symmetry. Its frequency is very close to the germanene mode analogous to the G mode of graphene [7,8], despite the large buckling of the germanium plane and the bonding with the neighboring Ga atoms. We find through our XRD measurements that a structural transition intervenes at ∼16 GPa. At this pressure Raman and IR signals vanish and do not reappear even at the highest measured pressure of 49.5 GPa. Electronic structure calculations show that this vanishing can be ascribed to the completely metallic nature of the new phase with the damping of Raman modes and loss of IR transmission. However, itinerant charge carriers already appear at a lower pressure at ∼6 GPa as seen by the changes in both Raman and IR signals, with calculations indicating a Fermi-level crossing of the valence band.

II. EXPERIMENTAL DETAILS

GaGeTe single crystals were made in a Bridgman furnace from polycrystalline GaGeTe synthesized from high-purity Ge, Ga, and Te. In all experiments, freshly cleaved GaGeTe was loaded in a membrane diamond anvil cell (DAC) [9] with neon as the pressure transmitting medium [10] and a ruby [11] for pressure calibration [12]. The powder XRD experiments under pressure (up to 17 GPa) were performed using an 80 μm beam at 25 keV ($\lambda = 0.4957$ Å) on the Xpress beamline at

*These authors contributed equally to this work.
†abhay.shukla@sorbonne-universite.fr

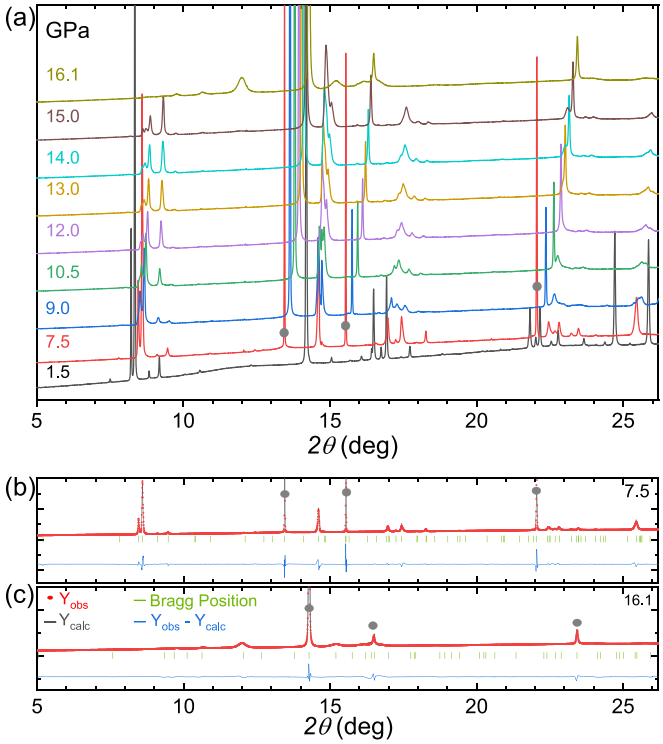

FIG. 1. (a) X-ray diffraction patterns of GaGeTe as a function of pressure. While the $R\bar{3}m$ structure remains unchanged until 15 GPa, at 16.1 GPa a new structural phase appears. (b) LeBail fit to the data at 7.5 GPa with the $R\bar{3}m$ structure. (c) LeBail fit to the data at 16.1 GPa with the $P3m1$ structure. The sharp Bragg peaks (gray solid circles) are from the crystallization of the pressure transmitter (neon).

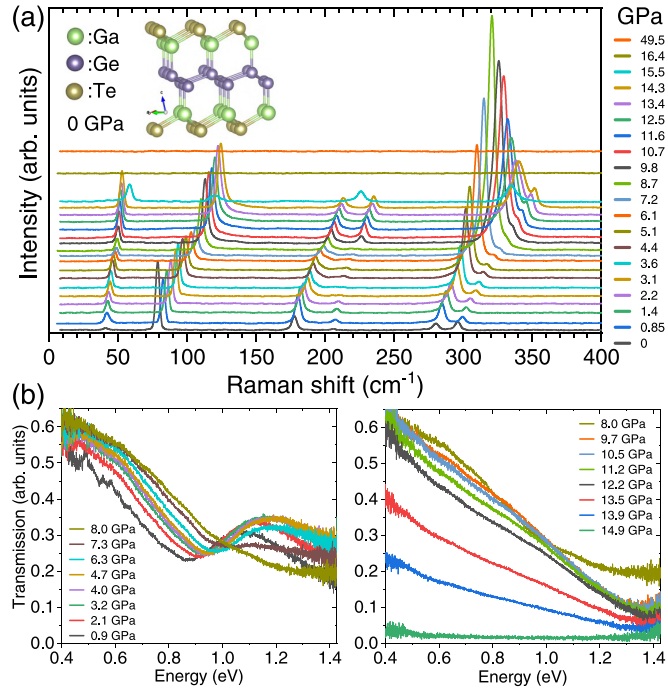

FIG. 2. (a) Raman spectra of GaGeTe as a function of pressure. Above 15.5 GPa the Raman signal disappears, signaling a strongly damped metallic state. The insets show the ambient pressure GaGeTe crystal structure. (b) IR transmission for GaGeTe over the same pressure range. Left panel: Transmission from 0.9 to 8 GPa pressure. Right panel: Transmission from 8 to 15 GPa.

the Elettra Sincrotrone (Trieste, Italy). Le Bail refinements (Fig. 1) were performed using FULLPROF28.

Raman scattering was performed in backscattering with a 514.5-nm Ar laser focused to a 2 μm spot with incident power limited below 40 mW. The 10 cm^{-1} low-frequency cutoff was achieved with three volume Bragg filters. A remnant low-energy tail was subtracted using a polynomial background. Data were recorded in the 10–1200 cm^{-1} range and a normalized count rate obtained. IR transmission was measured through a GaGeTe flake in a DAC using an in vacuum Fourier transform infrared spectrometer. Spectra were recorded in the 4000–11 000 cm^{-1} range with a tungsten source and spectral resolution of 4 cm^{-1}. Fabry-Pérot oscillations in the transmission spectra were filtered out with Fourier transform filtering for each spectrum. All measurements are at room temperature.

All simulations were performed with the QUANTUM ESPRESSO [13,14] codes using the local gradient approximation with Perdew-Burke-Ernzerhof (PBE) [15] parametrization. Atoms were modeled with scalar-relativistic norm-conserving pseudopotentials from the PseudoDojo project [16] with a kinetic energy cutoff of 80 Ry. Charge density was integrated over a reciprocal space grid of 8×8×8 points. When required, electronic occupations were modeled with a Methfessel-Paxton broadening of 0.02 Ry [17]. Phonon calculations were performed at the Γ point using density functional perturbation theory and Raman-active modes were identified by symmetry. Electronic bands are plotted along some high-symmetry directions.

III. RESULTS AND DISCUSSION

In Fig. 1(a), powder XRD data are shown from ambient pressure to 16.1 GPa. The ambient pressure phase persists almost throughout and is well fit with the $R\bar{3}m$ structure as shown in Fig. 1(b) for 7.5 GPa. At 16.1 GPa the XRD pattern undergoes a significant change and is compatible with the $P3m1$ structure [Fig. 1(c)]. We will discuss this structural change with respect to electronic structure calculations below. XRD data [18] show that with increasing pressure the sample undergoes texturing, degrading the quality of measurement [19]. At 16.1 GPa the new phase seems to be composed of only a few crystalline grains [18]. Spectroscopic measurements help to correlate the change in structure to the change in electronic properties.

In Fig. 2 we present results of Raman and IR measurements as a function of pressure. Six Raman peaks with non-negligible intensity are visible up to 14.3 GPa in Fig. 2(a). The spectrum at 15.5 GPa is considerably damped and above 16 GPa the Raman spectrum is a featureless flat background until the highest measured pressure of 49.5 GPa. The disappearance of the Raman signal at 16 GPa can be linked to the structural change found in the XRD measurements at the same pressure while the continuous presence of the six Raman peaks is coherent with the persistence of the ambient pressure phase below ∼16 GPa. Indeed, in this regime all peak

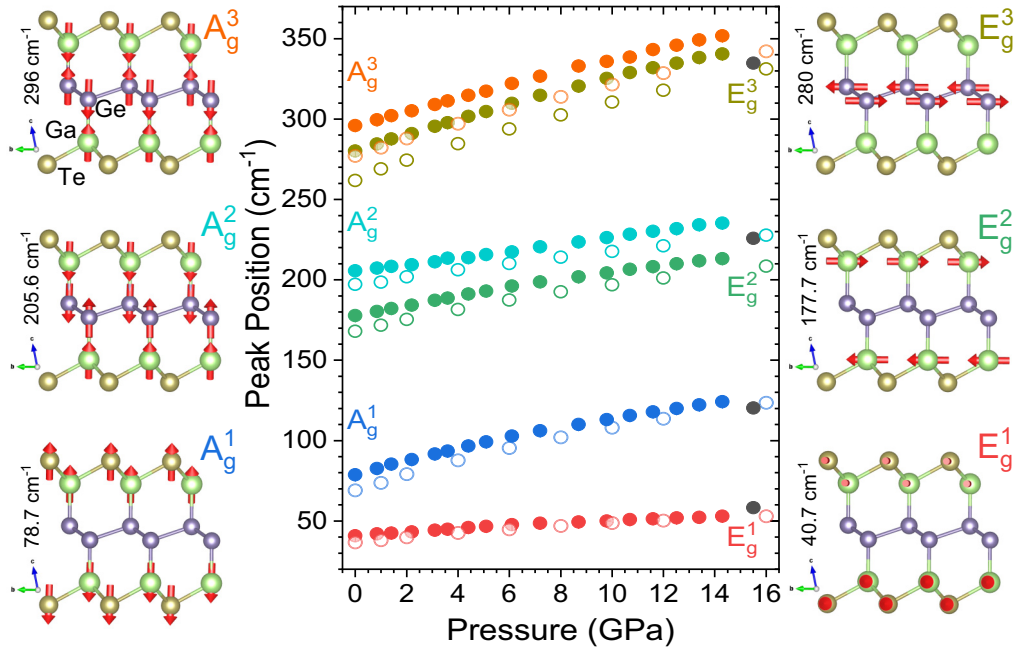

FIG. 3. The variation of the Raman modes with pressure. The measured frequencies (solid circles) are compared to the calculated *ab initio* values (open circles). The side panels show the atomic movements of the corresponding zone center phonons. Three modes with out-of-plane vibrations of atoms (A_g symmetry) and three more with in-plane vibrations of atoms (E_g symmetry) can be observed.

frequencies expectedly harden with pressure to varying degrees. There are considerable variations of intensities for the peak at 78.7 cm^{-1} and the one at 280 cm^{-1} (ambient condition frequencies) as pressure is increased. To confirm the nature of the transition at ∼16 GPa we also performed IR transmission measurements in the 0.4–1.4 eV range (4000–11 000 cm^{-1}) [Fig. 2(b)]. The lowest-pressure (0.9 GPa) transmission spectrum is in good agreement with an earlier ambient pressure measurement [20]. Up to a pressure of 8 GPa (left panel) the spectrum is characterized by decreasing transmission as energy increases, a minimum at around 1 eV and a small peak in transmission around 1.2 eV. When the same transmission data are plotted as a function of pressure for a given wave number it reveals an anomaly at 6 GPa [18]. Above 8 GPa (right panel) the transmitted intensity decreases with pressure over the whole energy range and above 15 GPa the transmission is zero. This zero transmission pressure also corresponds to the disappearance of the Raman signal.

In Fig. 3 the measured (solid circles) and calculated (open circles) variations of the Raman mode frequencies are plotted against the applied pressure. The side panels show the atomic movements of the corresponding zone center phonons [21]. The six modes are roughly grouped in three pairs of modes [6]. In these pairs, the lower-frequency mode is an in-plane vibration with E_g symmetry while the higher-frequency one is an out-of-plane vibration with A_g symmetry. The calculated *ab initio* frequencies as well as their variation with pressure are in excellent agreement with the experiment. No significant change either in the number of modes or the slope of the dispersion with pressure is observed, indicating that there is no structural phase transition in the measured range. At 15.5 GPa (solid black circles) the measured spectrum changes as the phonon modes are strongly damped and reduced in number. For higher pressure and up to the highest measured pressure of 49.5 GPa, Raman modes are no longer observed. Between 3 and 4 GPa the A_g^1 mode at 78.7 cm^{-1} evolves to an asymmetric line shape with an increasing linewidth as the pressure increases. This mode involves out-of-plane vibrations of Ga and Te atoms. Below (Fig. 5) we will show that the asymmetric line shape is a consequence of interference between the vibrational mode and continuum scattering from low-energy electron-hole pair excitations generated by a band crossing the Fermi level with additional pressure. The second mode of interest is the E_g^3 mode at 280 cm^{-1}. This mode involving in-plane vibrations of the Ge atoms is the analog of the graphene *G* mode for germanene [7,22]. The Ge plane in GaGeTe can be considered to represent buckled germanene. The mode shows considerable variations in intensity and width which we will examine in light of the changes in the electronic structure of GaGeTe with pressure.

As we have seen earlier, the *ab initio* Raman frequencies are in excellent agreement with the measurements. In Fig. 4(a) we show the evolution of the electronic structure as given by calculations at three key values of pressure: ambient, 6 GPa, and 16 GPa. The ambient-pressure electronic structure [22] shows a small direct band gap at the *R* point of the Brillouin zone (BZ) where both the dispersive valence band and the conduction band are close to the Fermi level. An indirect gap can be defined from the top of the valence band at the *R* point to two other points of the BZ, the bottom of the conduction band at Γ and at *M*. As pressure increases to 6 GPa, the top of the dispersive valence band at *R* approaches the Fermi level inducing delocalized charge carriers [Fig. 4(b)]. At 16 GPa our calculations indicate that both the $R\bar{3}m$ structure and a new $P3m1$ structure [23] are energetically possible, separated only by 40 meV. While the XRD data are incompatible with the $R\bar{3}m$ structure, we successfully fitted the data at this pressure with the $P3m1$ structure. As can be seen in Fig. 4(c), this phase

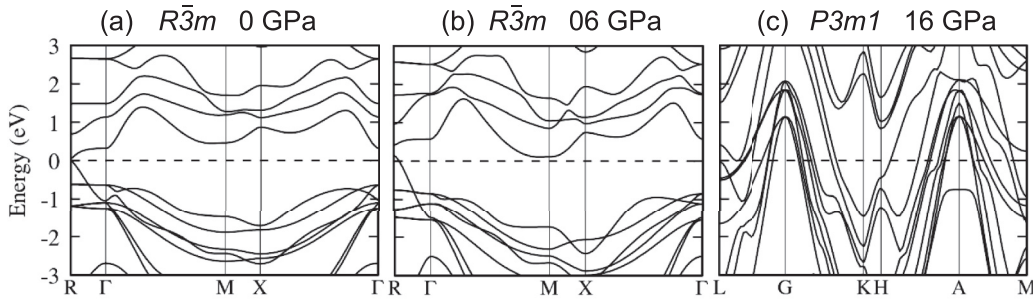

FIG. 4. Evolution of the first-principles-calculated electronic structure at three key values of the pressure: (a) ambient, (b) 6 GPa, and (c) 16 GPa.

is completely metallic. The vanishing Raman signal at 16 GPa and the total loss of the IR transmission can now be explained by strong damping with the sudden increase in carrier density after the phase transition.

We now discuss both the Raman and the IR data in more detail. The Raman response may become inactive because of the symmetry of the new phase if the transition is to a rocksalt structure [24]. This is ruled out by our XRD data and also by our calculations. Between 6 and 16 GPa the Raman signal persists even though free carriers exist (see Fig. 5) but it is completely damped by the transition to a strongly metallic phase at 16 GPa. Such damping has been observed in other systems showing metal-insulator transitions [25–27]. It may be argued that the nonzero IR transmission shown in Fig. 2(b)

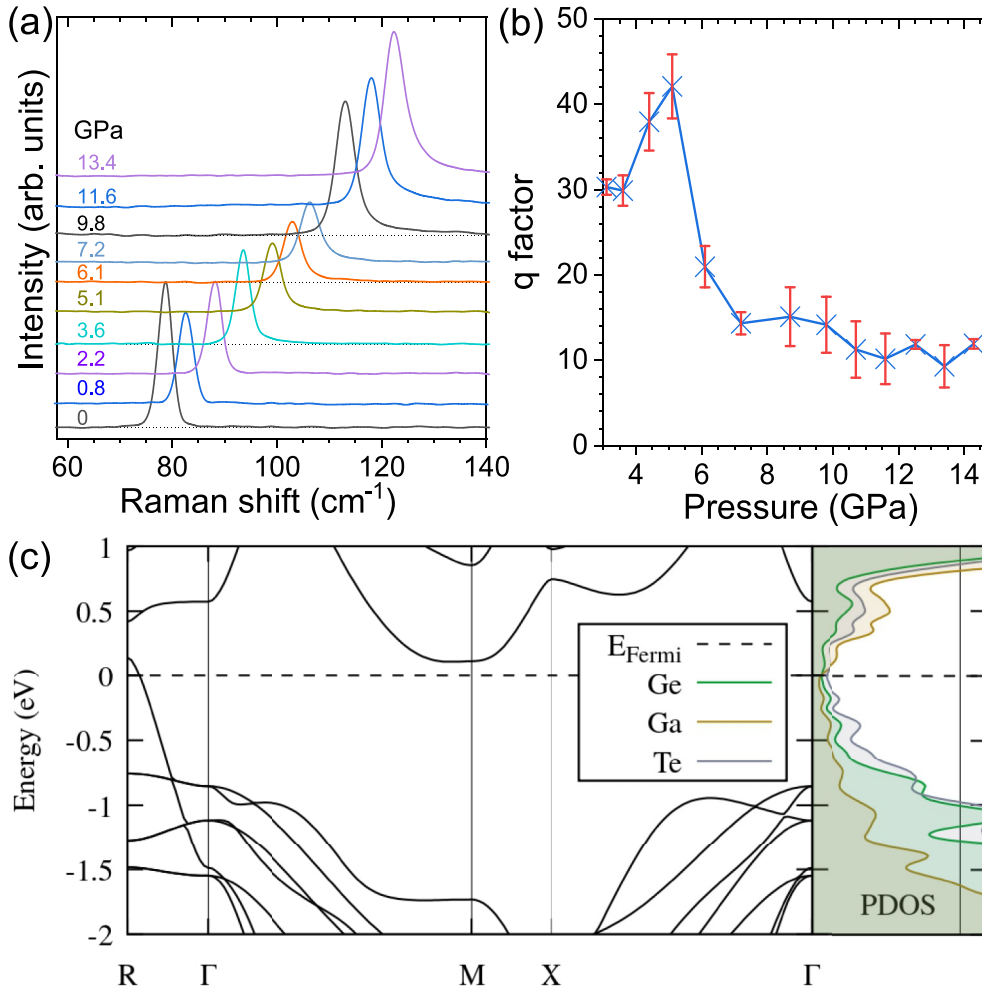

FIG. 5. (a) Variation of the A_g^1 mode with pressure showing the mode becoming wider and asymmetric at higher pressure. The baseline is shown for a few pressures. (b) q factor (signaling asymmetry) extracted from a Breit-Wigner-Fano line-shape fit. (c) Electronic structure and partial density of states at 6 GPa.

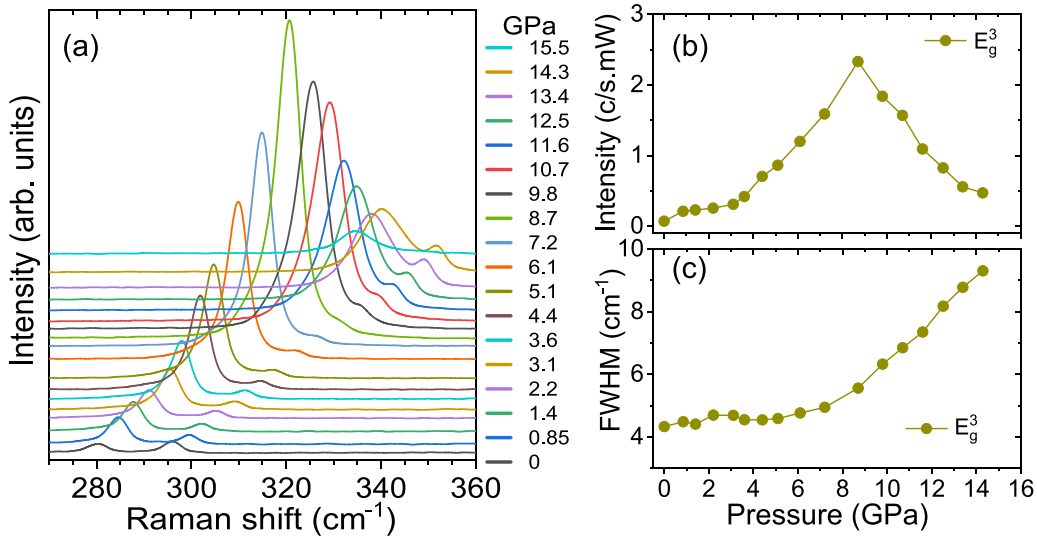

FIG. 6. (a) Variation of the E_g^3 mode with pressure. The E_g^3 mode for the Ge plane ("germanene") is analogous to the graphene G mode. (b) Intensity and (c) linewidth variation of the E_g^3 mode.

indicates an electronic structure with an ambient pressure gap of the order of an eV instead of a much smaller gap as found by calculations. However, the absolute transmission depends on the sample thickness which was not measured to avoid possible contamination by ambient exposure. Instead, several samples were tested until one with sufficient transmission was obtained. This sample is estimated to be less than 1 μm thick, consistent with the thickness estimation for a sample with a similar spectrum [20]. Indeed, even a sufficiently thin sample of graphite can transmit in the same range of energy [28] despite graphite having a vanishing gap. A final word of caution concerns the value of this direct gap at Γ. For GaGeTe it has been shown [1] that the calculated value can depend on the energy functional used and can vary between nearly zero to more than 0.5 eV.

We now examine the variation with pressure of the two Raman modes discussed briefly above. In Fig. 5(a) we show the variation of the A_g^1 mode. The line shape is symmetric and narrow at low pressure but becomes asymmetric and widens at higher pressures. This change is analyzed using an asymmetric Breit-Wigner-Fano line shape [Eq. (1)] to fit the measured peak [29],

$$I(\omega_s) = I_0\left[\frac{1}{q^2} + \frac{1 - 1/q^2}{1 + s^2} + \frac{2s/q}{1 + s^2}\right], \qquad (1)$$

where $s = (\omega_s - \omega_G)/\Gamma$, and ω_s, ω_G, q, Γ, and I_0 are the Raman shift, the spectral peak position, the asymmetry factor, the spectral width, and the maximum intensity of the peak, respectively. The lower the asymmetric factor q, the higher is the interference with the continuum excitations. Figure 5(b) shows that the q factor suddenly drops by a factor of 4 between 5 and 6 GPa, corresponding to the valence band crossing the Fermi level at the BZ R point in our calculations. In Fig. 5(c) the electronic structure at 6 GPa is shown around the Fermi level with the corresponding partial density of states of Ge, Ga, and Te. The states with the highest density around the Fermi level are those from Te. The A_g^1 vibration involves out-of-plane movements of Te and Ga, confirming that this particular mode couples to the relevant electronic states to generate the interference and modified line shape.

Finally, in Fig. 6(a) we show the variation of the E_g^3 mode with pressure. The E_g^3 mode is due to the in-plane vibration of Ge atoms and constitutes the germanene analog of the G mode for graphene [7,8]. The fact that this mode is seen throughout the pressure range implies that despite the large buckling the Ge plane retains its character, though the mode undergoes variations of intensity and width [Figs. 6(b) and 6(c)]. The intensity variations can be ascribed to resonant effects as the electronic structure varies with pressure. Lopez *et al.* [6] have shown that most Raman modes in GaGeTe at ambient pressure vary in intensity with the energy of the incident Raman light. In their work, the E_g^3 mode is nonresonant at an incident energy of 2.41 eV, corresponding to our incident energy, but shows a remarkable increase in intensity for an incident energy of 2.6 eV. In our experiment, the incident energy is constant but the electronic structure varies with pressure as seen in Fig. 4. It is probable that at 9 GPa, an electronic transition is resonant with our incident energy resulting in the maximum of intensity for the E_g^3 mode seen in Fig. 6(b). In Fig. 6(c) we observe that the linewidth of the E_g^3 mode is constant at low pressure but above 5–6 GPa it steadily increases. This can be due to increased anharmonicity or due to enhanced electronic scattering through electron-phonon coupling [30]. The simpler explanation is the latter since charge carriers which could scatter phonons become available at this pressure.

IV. CONCLUSION

In conclusion, in this paper we examine the pressure phase diagram of GaGeTe using x-ray diffraction, Raman and IR spectroscopy, and *ab initio* calculations. Earlier work has shown the advantages of studying the evolution of the

electronic structure in layered compounds such as MoS_2 [3,4] or BiTeI [5] with pressure. GaGeTe is a chalcogenide containing a germanene plane and an unusual rhombohedral structure. Under pressure, GaGeTe undergoes both electronic and structural transitions. Calculations indicate that delocalized charge carriers become available at ~ 6 GPa as the valence band approaches the Fermi level, a phenomenon that explains changes seen in the spectroscopic measurements. Above this pressure the Raman data indicate Fano coupling between a Raman mode and the charge continuum and IR spectra show uniformly decreasing transmission. At 16 GPa, the Raman signal disappears, IR transmission goes to zero and the diffraction data signal a transition to the $P3m1$ structure which calculations confirm to be completely metallic.

ACKNOWLEDGMENTS

This work was granted HPC resources of IDRIS under GENCI Project No. 7320. D.S.N. would like to thank DST for support via a Women Scientists fellowship (WOS-A) (Grant No. SR/WOS-A/PM-98/2018). O.F. acknowledges the support of the Czech Science Foundation Project No. 20-08633X.

[1] F. Pielnhofer, T. V. Menshchikova, I. P. Rusinov, A. Zeugner, I. Yu. Sklyadneva, R. Heid, K. Bohnen, P. Golub, A. I. Baranov, E. V. Chulkov, A. Pfitzner, M. Ruck, A. Isaeva *et al.*, J. Mater. Chem. C **5**, 4752 (2017).

[2] E. Haubold, A. Fedorov, F. Pielnhofer, I. P. Rusinov, T. V. Menshchikova, V. Duppel, D. Friedrich, R. Weihrich, A. Pfitzner, A. Zeugner *et al.*, APL Mater. **7**, 121106 (2019).

[3] A. P. Nayak, S. Bhattacharyya, J. Zhu, J. Liu, X. Wu, T. Pandey, C. Jin, A. K. Singh, D. Akinwande, and J.-F. Lin, Nat. Commun. **5**, 3731 (2014).

[4] Á. M. García, E. del Corro, M. Kalbac, and O. Frank, Phys. Chem. Chem. Phys. **19**, 13333 (2017).

[5] M. K. Tran, J. Levallois, P. Lerch, J. Teyssier, A. B. Kuzmenko, G. Autés, O. V. Yazyev, A. Ubaldini, E. Giannini, D. van der Marel, and A. Akrap, Phys. Rev. Lett. **112**, 047402 (2014).

[6] E. López-Cruz, M. Cardona, and E. Martinez, Phys. Rev. B **29**, 5774 (1984).

[7] E. Scalise, M. Houssa, G. Pourtois, B. Broek, V. Afanasev, and A. Stesmans, Nano Res. **5**, 43 (2013).

[8] H. S. Tsai, Y. Z. Chen, H. Medina, T. Y. Su, T. S. Chou, Y. H. Chen, Y. L. Chueh, and J. H. Liang, Phys. Chem. Chem. Phys. **17**, 21389 (2015).

[9] J. C. Chervin, B. Canny, J. M. Besson, and P. Pruzan, Rev. Sci. Instrum. **66**, 2595 (1995).

[10] B. Couzinet, N. Dahan, G. Hamel, and J. C. Chervin, High Press. Res. **23**, 409 (2003).

[11] J. C. Chervin, B. Canny, and M. Mancinelli, High Press. Res. **21**, 305 (2002).

[12] J. D. Barnett, S. Block, and G. J. Piermarini, Rev. Sci. Instrum. **44**, 1 (1973).

[13] P. Giannozzi, S. Baroni, N. Bonini, M. Calandra, R. Car, C. Cavazzoni, D. Ceresoli, G. Chiarotti, M. Cococcioni, I. Dabo *et al.*, J. Phys.: Condens. Matter **21**, 395502 (2009).

[14] Q. Giannozzi, O. Andreussi, T. Brumme, O Bunau, M. Buongiorno Nardelli, M. Calandra, R. Car, C. Cavazzoni, D. Ceresoli, M. Cococcioni *et al.*, J. Phys.: Condens. Matter **29**, 465901 (2017).

[15] J. P. Perdew, K. Burke, and M. Ernzerhof, Phys. Rev. Lett. **77**, 3865 (1996).

[16] M. van Setten, M. Giantomassi, E. Bousquet, M. J. Verstraete, D. R. Hamann, X. Gonze, and G.-M. Rignanese, Comput. Phys. Commun. **226**, 39 (2018).

[17] M. Methfessel and A. T. Paxton, Phys. Rev. B **40**, 3616 (1989).

[18] See Supplemental Material at http://link.aps.org/supplemental/10.1103/PhysRevB.109.054107 for x-ray diffraction data and analysis.

[19] E. Bandiello, S. Gallego-Parra, A. Liang, J. A. Sans, V. Cuenca-Gotor, E. Lora da Silva, R. Vilaplana, P. Rodríguez-Hernandez, A. Munoz, D. Diaz-Anitchenko, C. Popescu, F. G. Alabarse, C. Rudamas, C. Drasar, A. Segura, D. Errandonea, and F. J. Manjon, Mater. Today Adv. **19**, 100403 (2023).

[20] V. Kucek, C. Drasar, J. Navratil, L. Benes, and P. Lostak, J. Cryst. Growth. **380**, 72 (2013).

[21] K. Momma and F. Izumi, J. Appl. Cryst. **41**, 653 (2008).

[22] F.-B. Zheng, L. Zhang, J. Zhang, P.-J. Wang, and C. Zhang, Phys. Chem. Chem. Phys. **22**, 5163 (2020).

[23] S. Gallego-Parra, E. Bandiello, A. Liang, E. Lora da Silva, P. Rodríguez-Hernandez, A. Munoz, S. Radescu, A. H. Romero, C. Drasar, D. Errandonea, and F. J. Manjon, Mater. Today Adv. **16**, 100309 (2022).

[24] A. Pawbake, C. Bellin, L. Paulatto, K. Béneut, J. Biscaras, C. Narayana, D. J. Late, and A. Shukla, Phys. Rev. Lett. **122**, 145701 (2019).

[25] S. Zhang, J. Y. Chou, and L. J. Lauhon, Nano Lett. **9**, 4527 (2009).

[26] R. Naik B., D. Verma, and V. Balakrishnan, Appl. Phys. Lett. **120**, 062101 (2022).

[27] D. Kumar, M. Chandrana, and M. S. Ramachandra Rao, Appl. Phys. Lett. **110**, 191602(2017).

[28] J. B. Yasinsky and S. Ergun, Carbon **2**, 355 (1965).

[29] E. H. Hasdeo, A. R. T. Nugraha, M. S. Dresselhaus, and R. Saito, Phys. Rev. B. **90**, 245140 (2014).

[30] A. Shukla, M. Calandra, M. d'Astuto, M. Lazzeri, F. Mauri, C. Bellin, M. Krisch, J. Karpinski, S. M. Kazakov, J. Jun, D. Daghero, and K. Parlinski, Phys. Rev. Lett. **90**, 095506 (2003).